Particle Breakage of Rockfill Material during Triaxial Tests under Complex Stress Paths

Yufeng Jia[1]; Bin Xu[2]; Shichun Chi[3]; Biao Xiang[4]; Dai Xiao[5]; and Yang Zhou, Ph.D.[6]

Abstract: Particle breakage modifies the structure of rockfill material and influences its constitutive character, which is the key factor in earth-rockfill dam deformation control. However, the particle breakage laws for rockfill material under real stress paths during dam construction and impounding remain unclear. This paper investigates the particle breakage of basalt rockfill, which was used in the Gushui concrete-face rockfill dam, during drained triaxial compression under equal stress ratio paths (construction stress paths) and transitional stress paths (impounding stress paths). The results indicate that the type of stress path significantly influences rockfill particle breakage. Under the equal stress ratio path, particle breakage increases with shear strain and the growth rate decreases with the stress ratio. The relationship between the relative particle breakage index and the plastic work can be simulated using a hyperbolic formulation. Under the transitional stress path, particle breakage also increases with shear strain and the growth rate is influenced by the transitional confining pressure, the transitional stress path, and the equal stress ratio experienced before the transition. However, the relative particle breakage index cannot be reasonably simulated using the plastic work. **DOI: 10.1061/(ASCE)GM.1943-5622.0001517.** © *2019 American Society of Civil Engineers.*

Author keywords: Complex stress path; Particle breakage; Rockfill material; Relative particle breakage.

Introduction

With the development of rolled earth–rockfill dams, many earth-rockfill dams with heights greater than 200 m and even reaching 300 m have been constructed or are under construction, including the Shuangjiangkou core-wall rockfill dam (312 m, under construction on the Dadu River in Sichuan Province, China), the Changheba core-wall rockfill dam (240 m, constructed on 79.3-m-thick riverbed alluvium on the Dadu River in Sichuan Province, China), the Shuibuya concrete-face rockfill dam (CFRD) (233 m, constructed on the Qingjiang River in Hubei Province, China), and the Nuozhadu core-wall rockfill dam (261.5 m, constructed on the Lancang River, Yunan Province, China). Deformation control is a central problem in the design and operation of these high or superhigh earth-rockfill dams. The constitutive model of the rockfill, which is the main material used in dam engineering, determines the accuracy of the earth-rockfill deformation analysis. However, with increasing dam height, the rockfill experiences greater stress, which is generated by gravity and water pressure and produces significant particle breakage. The particle breakage modifies the rockfill structure directly, influencing its dilatancy, friction angle, strength, and permeability, as well as generating creep deformation, wetting deformation, and residual deformation under a seismic load (Jia et al. 2017).

In recent decades, many researchers have performed laboratory tests to investigate the relationship between rockfill particle breakage and constitutive character (Chavez and Alonso 2003; McDowell 2003; McDowell and Bolton 1998; Oldecop and Alonso 2001; Salim and Indraratna 2004; Sun et al. 2014; Zhang et al. 2015), the factors that affect rockfill particle breakage generation (Guo et al. 1997; Sun et al. 2014; Xiao et al. 2014, 2016), and the rules of rockfill particle breakage under various loadings (Hardin 1985; Indraratna et al. 2013; Marachi et al. 1972; Marsal 1967; Qin et al. 2015; Wang et al. 2009; Wei and Zhu 2006; Yang et al. 2010a, b; Zhang et al. 2012). However, previous studies primarily focused on the amount of particle breakage before and after laboratory testing; thus, rockfill particle breakage during testing is still not well understood. Moreover, most tests were conventional consolidated-drained (CD) triaxial compression tests, one-dimensional compression tests, and dynamic triaxial tests. However, the loading stress paths of the rockfill specimens tested were different from the real stress paths of the rockfill used in dams.

Monitoring data (Charles 1976; Wei 2012) and numerical analysis results using the finite-element method (FEM) (Bai et al. 1999; Zhu et al. 2010) have shown that the stress path of rockfill in a dam approximates a constant stress ratio during dam construction and that it undergoes a transition during reservoir-filling (Chang and Zhang 2013; Feng et al. 2016; Xiang et al. 2009; Xiao et al. 2011). This indicates that the rockfill in the dam experiences a complex stress path loading that is an equal stress ratio path during construction and a transitional stress path during impounding. The stress path has been shown to have a notable influence on the constitutive character of rockfill (Chen et al. 2016; Liu et al. 2018; Ng et al. 2004; Ng 2005; Xiang et al. 2010). However, few complex stress path particle breakage tests for rockfill have been reported. Yuan et al. (2017) conducted a series of rockfill particle breakage tests to study particle breakage of quartz andesite rockfill under complex

[1]Lecturer, State Key Laboratory of Coastal and Offshore Engineering, Dalian Univ. of Technology, Dalian, Liaoning 116024, China. Email: jiayf130@dlut.edu.cn

[2]Associate Professor, School of Hydraulic Engineering, Dalian Univ. of Technology, Dalian, Liaoning 116024, China. Email: Xubin@dlut.edu.cn

[3]Professor, State Key Laboratory of Coastal and Offshore Engineering, Dalian Univ. of Technology, Dalian, Liaoning 116024, China (corresponding author). Email: Schchi@dlut.edu.cn

[4]Associate Professor, Hydraulic School, Yunnan Agricultural Univ., Kunming 650000, China. Email: 103931114@qq.com

[5]Engineer, SIPPR Engineering Group Co., Ltd., No. 191, Zhongyuanzhong Rd., Zhengzhou 450000, China. Email: 6473004@qq.com

[6]Lecturer, State Key Laboratory of Coastal and Offshore Engineering, Dalian Univ. of Technology, Dalian, Liaoning 116024, China. Email: Zhouy@mail.dlut.edu.cn

Note. This manuscript was submitted on August 25, 2018; approved on April 26, 2019; published online on October 1, 2019. Discussion period open until March 1, 2020; separate discussions must be submitted for individual papers. This paper is part of the ***International Journal of Geomechanics***, © ASCE, ISSN 1532-3641.

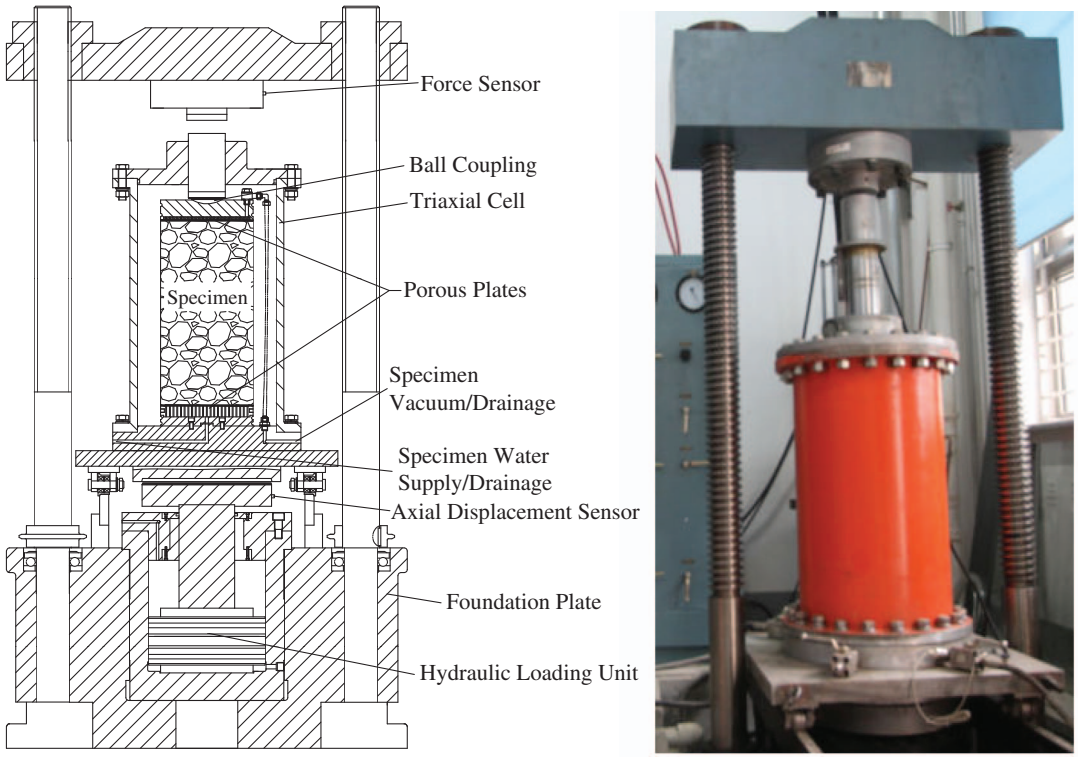

Fig. 1. (Color) Schematic of the large triaxial apparatus. (Reprinted from Jia et al. 2017, © ASCE.)

stress paths, but their focus was only on particle breakage before and after the tests and only one equal stress ratio path was applied during testing. The particle breakage laws for rockfill during deformation under different equal stress ratio paths and different transitional stress paths are still unclear.

This paper focuses on rockfill particle breakage during shearing in CD triaxial compression tests under complex stress paths. The rockfill would be used as the main rockfill in the Gushui CFRD, which was designed with a height of 242 m. A series of triaxial tests under the equal stress ratio path and the transitional stress path were performed to investigate rockfill particle breakage.

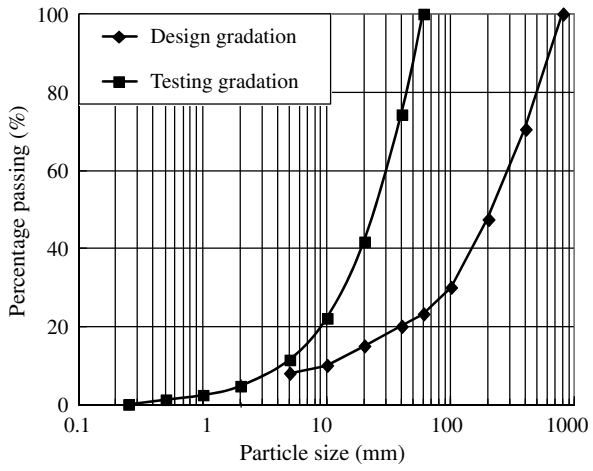

Fig. 2. Rockfill gradation used in the tests. (Reprinted from Jia et al. 2017, © ASCE.)

Testing Apparatus and Material

Triaxial compression tests under complex stress paths were conducted using a large-scale multifunctional triaxial apparatus developed by Dalian University of Technology which accommodates specimens 300 mm in diameter and 600 mm high. A schematic of the device is shown in Fig. 1. The largest axial load applied was 1,500 kN (6 MPa), the largest confining pressure was 3 MPa, and both load and pressure could be applied by controlling either the displacement or the force. The volumetric strain of the specimen was obtained by measuring the specimen's outgoing or incoming water volume using a high-precision scale sensor.

The rockfill material used in the test was basalt obtained from the Gushui quarry in Yunnan Province. Basalt rockfill has a specific gravity of 2.79; the compressive strength of the parent rock is 83.5 MPa. Fig. 2 shows the gradation of rockfill used in the tests. Specimen dry density was 2.21 g/cm^3, and the initial void ratio was 0.262.

Loading Stress Paths in the Complex Stress Path Tests

Loading stress paths in the complex stress path tests were determined according to the rockfill stress paths, calculated using FEM, in positions typical for an earth-rockfill dam. Fig. 3 shows these positions in the finite-element model of the Nuozhadu core-wall rockfill dam. Fig. 4 shows the calculated stress paths of the typical positions in four earth-rockfill dams; p is volumetric stress; and q is deviatoric stress.

According to the calculated stress paths shown in Fig. 4, the typical loading stress paths in the complex stress path tests were

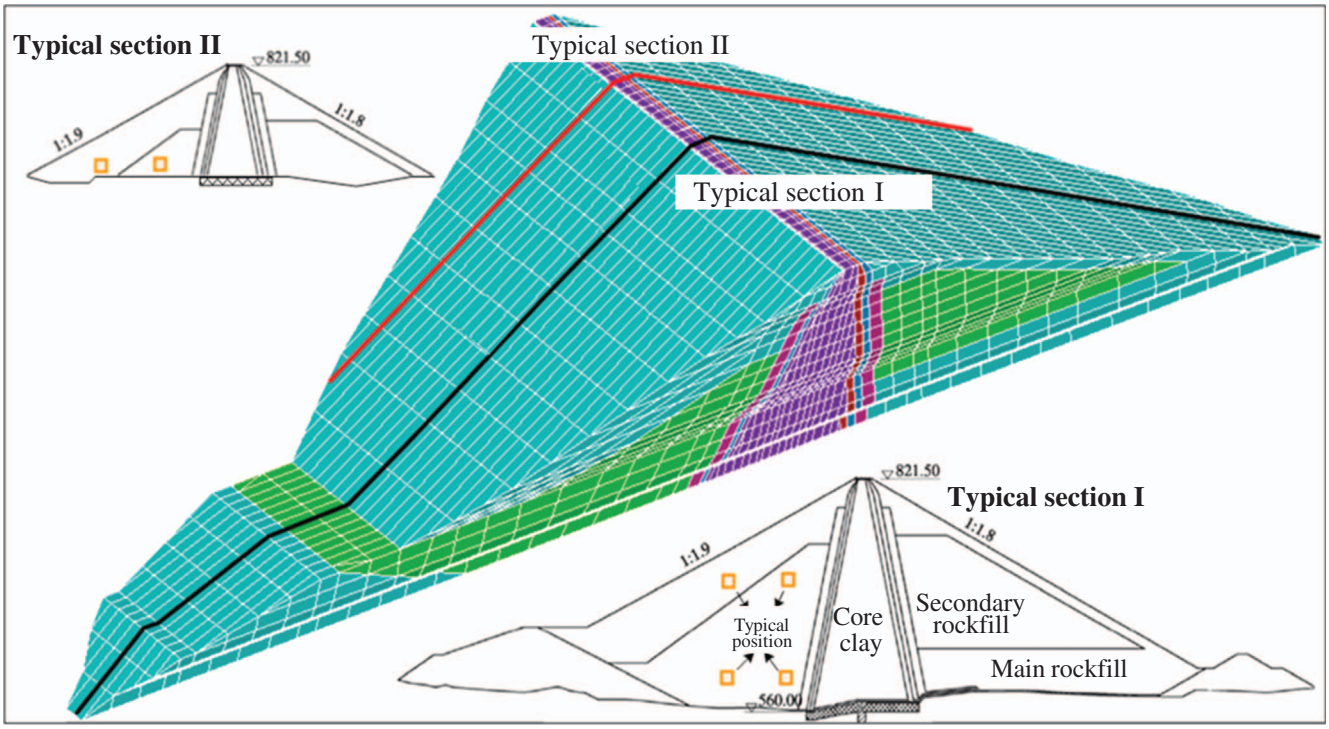

Fig. 3. (Color) Typical positions of the stress path calculations in the finite-element model.

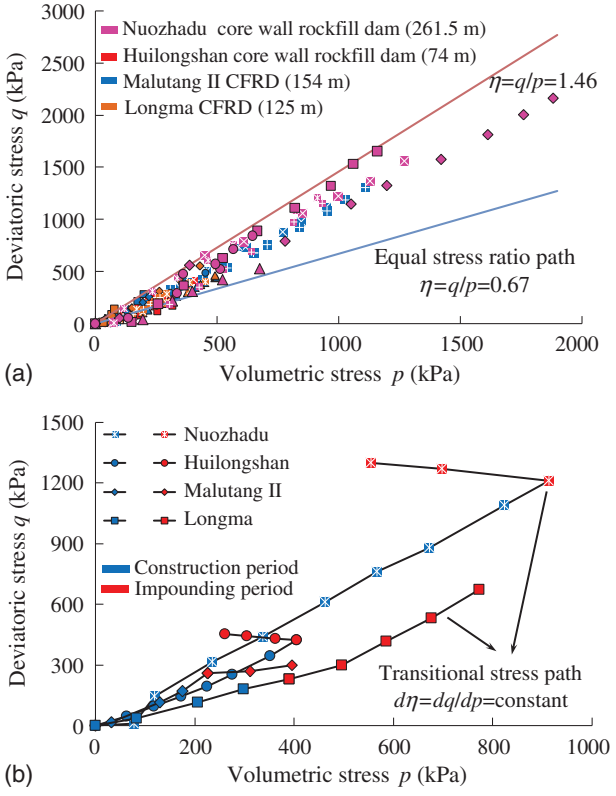

Fig. 4. (Color) Calculated stress paths of rockfill in earth-rockfill dams: (a) construction; and (b) impounding.

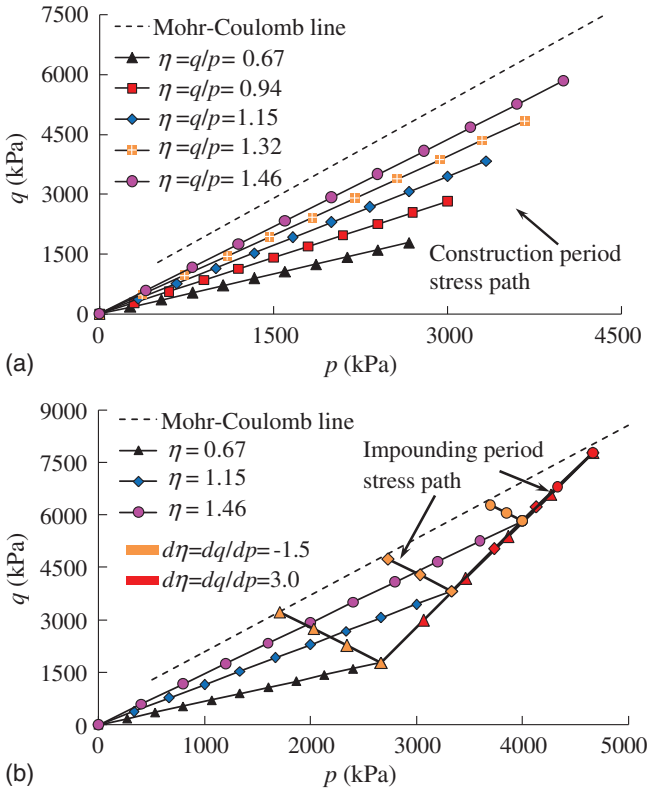

Fig. 5. (Color) Loading stress paths in the rockfill complex stress path tests: (a) equal stress ratio; and (b) transitional stress.

determined and are shown in Fig. 5. Fig. 5(a) shows that, under the equal stress ratio path, which simulates rockfill stress paths during dam construction, the specimens were sheared under five equal stress ratios: $\eta = q/p$ of 0.67, 0.94, 1.15, 1.32, and 1.46. Fig. 5(b) shows that the transitional stress path $d\eta = dq/dp$, which experienced equal stress ratios of 0.67, 1.15, and 1.46 before transition, were −1.5 and 3.0. Table 1 lists all complex stress path tests in detail.

Test Program and Test Procedures

The basalt rockfill particle breakage tests just discussed, which had been conducted by the authors, showed that specimen preparation generated notable particle breakage (Jia et al. 2017). In order to accurately measure rockfill particle breakage in specimen preparation, under equal stress ratio path shearing, and under transitional stress path shearing, three tests were performed: specimen preparation, CD triaxial compression under the equal stress ratio path, and CD triaxial compression tests under the transitional stress path.

Specimen Preparation Test

The specimen was compacted inside a 5-mm-thick rubber membrane placed in a split cylindrical mold. The rockfill was mixed and compacted in six layers using a vibratory hammer at a dry density of 2.21 g/cm^3. The specimen was dried and sieved after compaction and the particle breakage generated by compaction was obtained.

CD Triaxial Compression Tests under the Equal Stress Ratio Path

A new specimen was prepared, using new rockfill, as described previously. After compaction, the specimen was pushed into the triaxial cell and saturated under 30-kPa confining pressure. Then CO_2 was introduced from the bottom plate to replace the air in the specimen before saturation. The specimen was consolidated according to the loading stress ratio $\eta = q/p$ once saturation was higher than 95%. The resulting loading stress ratios η and unloading confining pressures σ_{3u} are listed in Table 1 for Loading paths 1through 8. In the consolidation, the water was drained from the plates at the bottom and top of the specimen, and the confining pressure was increased from 30 to 50 kPa. Shearing stress was also increased together with the loading stress ratio, which ensured that the specimen stress state accorded with the loading stress ratio, and little particle breakage appeared in the consolidation. After the drained water stabilized, the specimen was loaded to the unloading confining pressure, (Table 1), at an axial stress rate of 1 kPa/s under the equal stress ratio path. Once the unloading confining pressure was reached, the specimen was unloaded, dried, and sieved, and the particle breakage generated by compaction and shearing under the equal stress ratio path was obtained.

Table 1. Loading stress paths in the tests

Loading path No.	Equal stress ratio path, $\eta = q/p$	Unloading or transition confining pressure, σ_{3u} or σ_{3t} (kPa)	Transitional stress path, $d\eta = dq/dp$	Unloading shear strain, ε_s (%)
1	0.67	1,000	—	—
2	0.67	2,000	—	—
3	0.94	2,000	—	—
4	1.15	1,000	—	—
5	1.15	2,000	—	—
6	1.32	2,000	—	—
7	1.46	1,000	—	—
8	1.46	2,000	—	—
9	0.67	2,000	3.0	7.49[a]
10	0.67	2,000	3.0	13.47
11	0.67	1,000	3.0	14.52
12	1.15	2,000	3.0	8.35[a]
13	1.15	2,000	3.0	13.30
14	1.15	1,000	3.0	14.56
15	1.46	2,000	3.0	8.98[a]
16	1.46	2,000	3.0	13.31
17	1.46	1,000	3.0	14.56
18	0.67	2,000	−1.5	2.15[a]
19	0.67	2,000	−1.5	16.27
20	0.67	1,000	−1.5	17.95
21	1.15	2,000	−1.5	4.00[a]
22	1.15	2,000	−1.5	15.02
23	1.15	1,000	−1.5	17.12
24	1.46	2,000	−1.5	8.37[a]
25	1.46	2,000	−1.5	14.38
26	1.46	1,000	−1.5	16.07

[a]Peak shear strength occurred.

CD Triaxial Compression Tests under the Transitional Stress Path

A new specimen, with new rockfill, was prepared and sheared under the equal stress ratio path according to the methods described for the equal stress ratio path tests. After the loading confining pressure η reached the transition confining pressure σ_{3t}, the specimen was compressed under a transitional stress path $d\eta = dq/dp$ to a given shear strain. Loading was applied at an axial strain rate of 0.5 mm/min. The compression test was terminated when the axial strain reached 15% or the shear stress reached peak values. Fig. 6 shows the stress-strain curves under the equal stress ratio path ($\eta = 0.67$) at different unloading confining pressures ($\sigma_{3u} = 1{,}000$ and 2,000 kPa) and the corresponding transitional stress path ($d\eta = dq/dp = 3.0$), which were compressed under the same equal stress ratio path before the loading stress path changed at the transitional confining pressure ($\sigma_{3t} = 2{,}000$ kPa) and unloaded at two shear strains ($\varepsilon_s = 7.49\%$ and 13.47%). After the unloading shear strains were reached, the specimens were unloaded, dried, and sieved and the particle breakage factors at various shear strains were obtained., rockfill particle breakage during triaxial shearing under the transitional stress path could now be measured. Table 1 provides the initial loading equal stress ratio $\eta = q/p$, the transitional confining pressure σ_{3t}, the transitional stress path $d\eta = dq/dp$, and the unloading shear strain ε_s of Transitional stress paths 9 through 26.

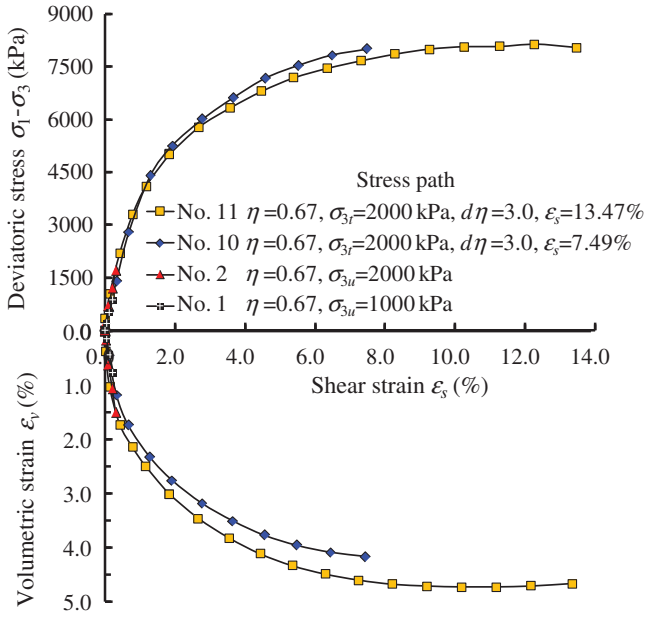

Fig. 6. (Color) Complex stress path stress-strain curves under an equal stress ratio of 0.67.

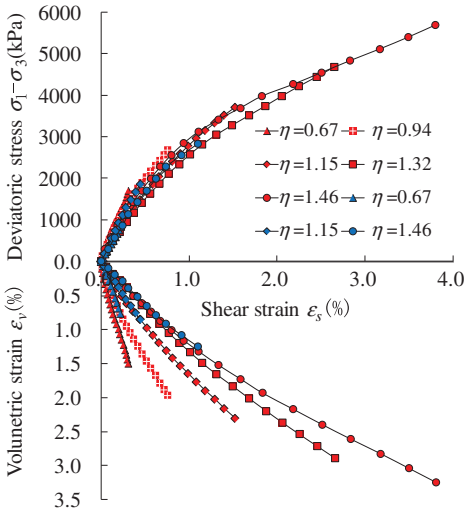

Fig. 7. (Color) Stress-strain curves under equal stress ratio paths.

Test Results

Particle Breakage in the CD Triaxial Tests under the Equal Stress Ratio Path

Stress-strain curves under equal stress ratio paths are shown in Fig. 7. The confining pressure changed under the complex stress path, and the volumetric strain was significantly influenced by penetration of the rubber membrane. Therefore, the volumetric strains in Fig. 7 were corrected using the method developed by Newland and Allely (1959). Fig. 7 shows that the slopes of the q–ε_s and ε_v–ε_s curves decreased with stress ratios η. In contrast, shear strain under the same unloading confining stress increased with η. These results accorded with the tests results for other rockfill materials (Xiang et al. 2009; Yuan et al. 2017).

Table 2 lists rockfill gradations before and after specimen preparation and CD triaxial testing under equal stress ratio paths. According to the table, the relative particle breakage index B_r, defined by Hardin (1985), was used to measure particle breakage. Table 3 provides the B_r index under each stress path and the corresponding volumetric strains ε_v, shear strains ε_s, and deviatoric stresses q.

On the basis of the test results provided in Table 3, the relative breakage index B_r and the shear strain ε_s under conventional triaxial stress paths and equal stress ratio paths are plotted in the p–q coordinate system in Fig. 8. The blue lines and data points represent conventional triaxial stress paths and maximum shear stress before unloading under each shear strain, respectively; the red lines and points indicate these values for equal stress ratio paths. Conventional test results from Jia et al. (2017) under confining pressures of 1,000 and 2,000 kPa were selected for comparison with the equal stress ratio path test results, which were derived from the same confining pressure.

Fig. 8 shows that the B_r under an equal stress ratio $\eta = 1.15$ and an unloading confining pressure $\sigma_{3u} = 2{,}000$ kPa was 1.53. This was far greater than the B_r of 0.96 under a conventional stress path at the same confining pressure. However, the shear strain ε_s for the former, 1.52, was much less than the shear strain ε_s for the latter, 1.85. Similarly, deviatoric stress q for the former was less than that

Table 3. B_r under each stress ratio

Loading path No.	η	σ_{3u} (kPa)	B_r (%)	ε_v (%)	ε_s (%)	q (kPa)
1	0.67	1,000	0.02	0.76	0.22	859
2	0.67	2,000	0.32	1.50	0.31	1,705
3	0.94	2,000	0.75	1.97	0.76	2,685
4	1.15	1,000	0.13	0.85	0.45	1,869
5	1.15	2,000	1.53	2.31	1.52	3,710
6	1.32	2,000	2.13	2.89	2.65	4,695
7	1.46	1,000	0.39	1.25	1.10	2,839
8	1.46	2,000	2.73	3.25	3.80	5,696

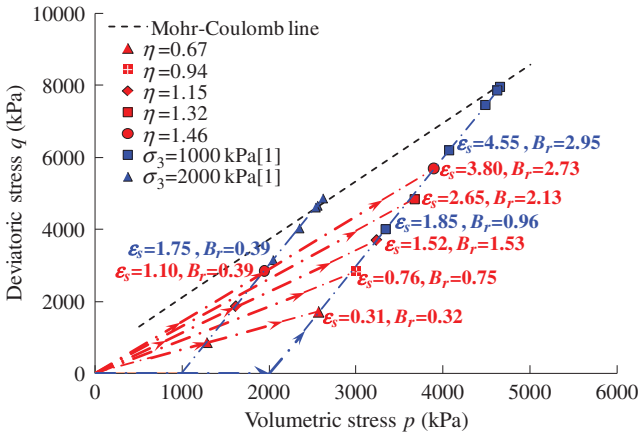

Fig. 8. (Color) B_r under conventional stress paths (data from Jia et al. 2017) and equal stress ratio paths.

Table 2. Rockfill gradation after CD triaxial tests under equal stress ratio paths

	Particle amount (%) at each grain group (mm)								
Status	40–60	20–40	10–20	5–10	2–5	0.5–2.0	0.25–0.5	0.075–0.25	<0.075
Before test	25.77	32.59	19.60	10.65	6.71	3.46	1.22	—	—
After specimen preparation	21.17	34.85	18.87	11.33	7.43	4.19	1.13	0.37	0.66
Loading path No.									
1	20.39	34.54	19.91	11.53	7.74	3.92	1.07	0.32	0.58
2	20.39	35.55	18.20	11.90	7.37	4.30	1.17	0.40	0.72
3	19.95	34.93	18.08	12.25	8.50	3.90	1.13	0.44	0.82
4	19.83	35.06	19.77	11.60	7.86	3.94	1.08	0.31	0.55
5	18.05	35.25	18.91	12.18	8.71	4.35	1.23	0.47	0.85
6	16.20	35.94	19.47	12.03	9.25	4.45	1.27	0.52	0.87
7	19.75	34.90	19.64	11.45	8.14	4.00	1.16	0.35	0.61
8	15.37	35.55	19.69	11.85	10.3	4.45	1.31	0.56	0.92

Int. J. Geomech., 2019, 19(12): 04019124

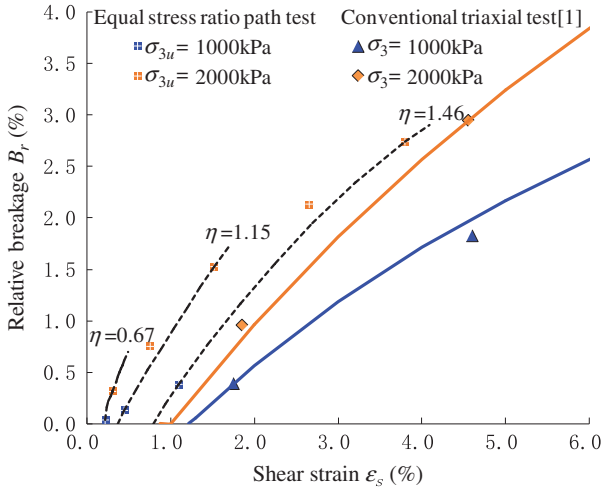

Fig. 9. (Color) B_r under different loading stress paths.

for the latter. A similar phenomenon appeared between the B_r under an equal stress ratio $\eta = 1.46$ and $\sigma_{3u} = 1{,}000$ kPa and the B_r under the conventional stress path at 1,000-kPa. For the former, ε_s was 1.10; for the latter, it was 1.75. The B_r value for both the former and the latter was 0.39. Furthermore, the B_r under an equal stress ratio $\eta = 0.94$ and $\sigma_{3u} = 2{,}000$ kPa was 0.75, which was much larger than the B_r of 0.39 under the conventional stress path at 1,000 kPa; the former ε_s at 0.76 was much less than the latter ε_s at 1.75. In summary, the rockfill under some equal stress ratio paths, which generated less shear strain ε_s and underwent less deviatoric stress q, generated a larger relative particle breakage factor B_r than the rockfill under a conventional stress path. However, particle breakage tests for the conventional stress path performed by the authors showed that both shear strain and stress affected particle breakage during shearing; the B_r at a given shear strain increased with deviatoric stress, and rockfill under lower deviatoric stress and higher shear strain generated larger B_r than rockfill under higher shear stress and lower shear strain (Jia et al. 2017). It is therefore concluded the loading stress path significantly influences rockfill particle breakage, which leads to a particle breakage law different from the laws for conventional stress paths.

On the other hand, B_r under an equal stress ratio $\eta = 1.46$ and a σ_{3u} of 2,000 kPa was 2.73, whereas ε_s was 3.8. This B_r was less than the B_r of 2.95 under a conventional stress path at 2,000 kPa confining pressure, which experienced an ε_s of 4.55. This result shows that under certain conditions, particle breakages under different stress paths obey the law that greater shear strain and stress generate more particle breakage. Therefore, the stress path's influence on particle breakage is not dominant but can be changed by shear strain and stress.

Fig. 9 shows the relationship between B_r and ε_s under different loading stress paths. Under an equal stress ratio path, B_r increased with ε_s and the growth rate increased as stress ratio η decreased. Under an equal stress ratio path, deviatoric stress q increased with ε_s and the growth rate increased as η decreased, as shown in Fig. 7. Under the conventional stress path, q also increased with ε_s and the growth rate increased with confining pressure. Therefore, Figs. 7 and 9 show that, under both equal stress ratio and conventional stress paths, deviatoric stress q and shear strain ε_s affect particle

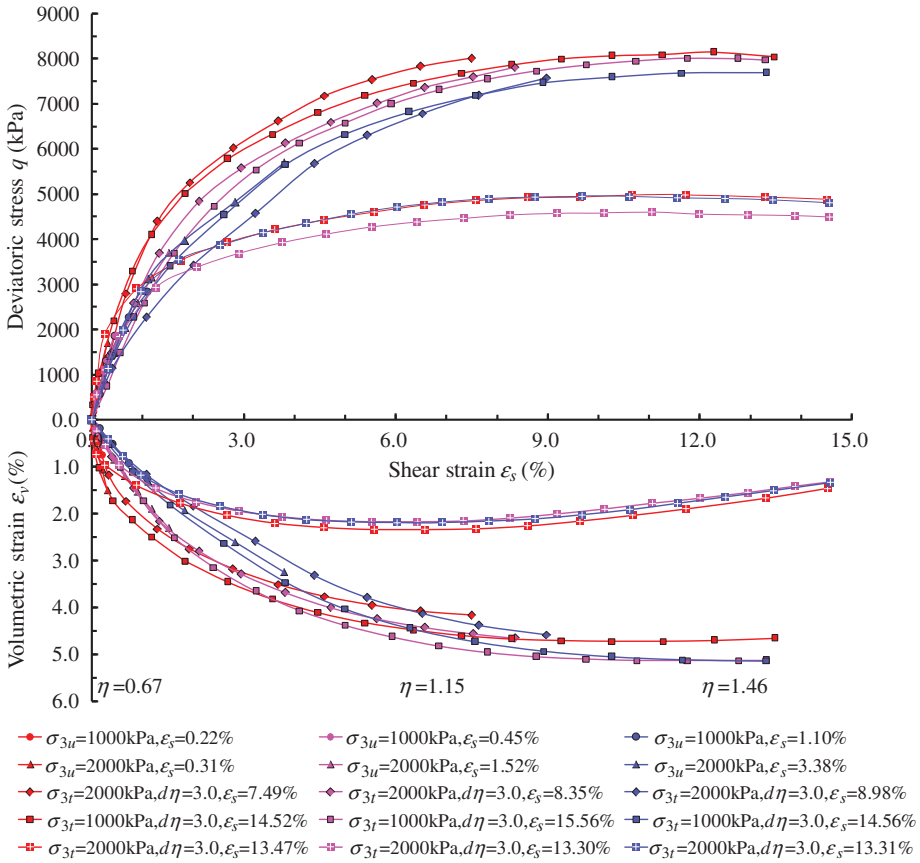

Fig. 10. (Color) Stress-strain curves under a transitional stress path of $d\eta = 3.0$.

breakage, and this effect is influenced by the loading stress path. Fig. 9 shows that, under an equal stress ratio path, no particle breakage occurred for some shear strain values (marked ε_{si}) at the beginning of the loading, which was also the case with the conventional stress path (Jia et al. 2017), and that ε_{si} decreased with η.

Particle Breakage in the CD Triaxial Tests under the Transitional Stress Paths

The stress-strain curves under transitional stress paths are shown in Figs. 10 and 11, which indicate that the transitional stress paths $d\eta = dq/dp$ equaled 3.0 and -1.5, respectively. The stress-strain curves under the equal stress ratio paths, corresponding to the loading stress ratio of the transitional stress path curves before the stress path transition, are shown in Figs. 10 and 11 for comparison.

Fig. 10 shows that, before the stress path transition, the stress-strain curves of the transitional stress path tests agreed well with the stress-strain curves under the same equal stress ratio path. The tangent stiffness of the stress-strain curves under a stress ratio of 0.67 was the largest and under a stress ratio of 1.46 was the smallest. However, after the stress path transition, the stress-strain curves of the transitional stress path tests under the same transitional confining pressure ($\sigma_{3t} = 1{,}000$ or 2,000 kPa), which experienced different equal stress ratio path loading and generated obviously different stress-strain curves, converged quickly. Furthermore, the convergence of the stress-strain curves for $\sigma_{3t} = 1{,}000$ kPa was higher than that for $\sigma_{3t} = 2{,}000$ kPa. The volumetric strain curves also obeyed these laws. Moreover, the stress-strain curves for $\sigma_{3t} = 2{,}000$ kPa reflected higher deviatoric stress than those for 1,000 kPa; the volumetric strain curves for $\sigma_{3t} = 2{,}000$ kPa indicated shearing contraction, and the volumetric strain curves for $\sigma_{3t} = 1{,}000$ kPa indicated obvious dilatancy. These results were similar to the conventional triaxial test results.

Fig. 11 shows that, before the transition, the stress-strain curves and volumetric curves of the transitional stress path tests also agreed with the curves under the same equal stress ratio path, as Fig. 10 shows. However, after the transition the stress-strain curves under the same transitional confining pressure ($\sigma_{3t} = 1{,}000$ or 2,000 kPa), which experienced different equal stress ratio path loading and transferred to the same stress path of $d\eta = dq/dp = -1.5$, were significantly different.

Fig. 11 shows that the specimens that experienced higher equal stress ratio η or larger transitional confining pressure σ_{3t} generated larger deviatoric stress. This result was different from that for the stress-strain curves under a transitional stress path of $d\eta = 3.0$ in Fig. 10. The volumetric strain curves followed similar laws: under 2,000-kPa transitional confining pressure, they showed obvious dilatancy and the 1,000-kPa curves generated more significant dilatancy.

Differences in the stress-strain and volumetric strain curves in Figs. 10 and 11 show that the influences of transitional stress path $d\eta = dq/dp$ and transitional confining pressure σ_{3t} on the constitutive character of rockfill material are complex and determined by the rockfill's transitional stress path and particle breakage laws.

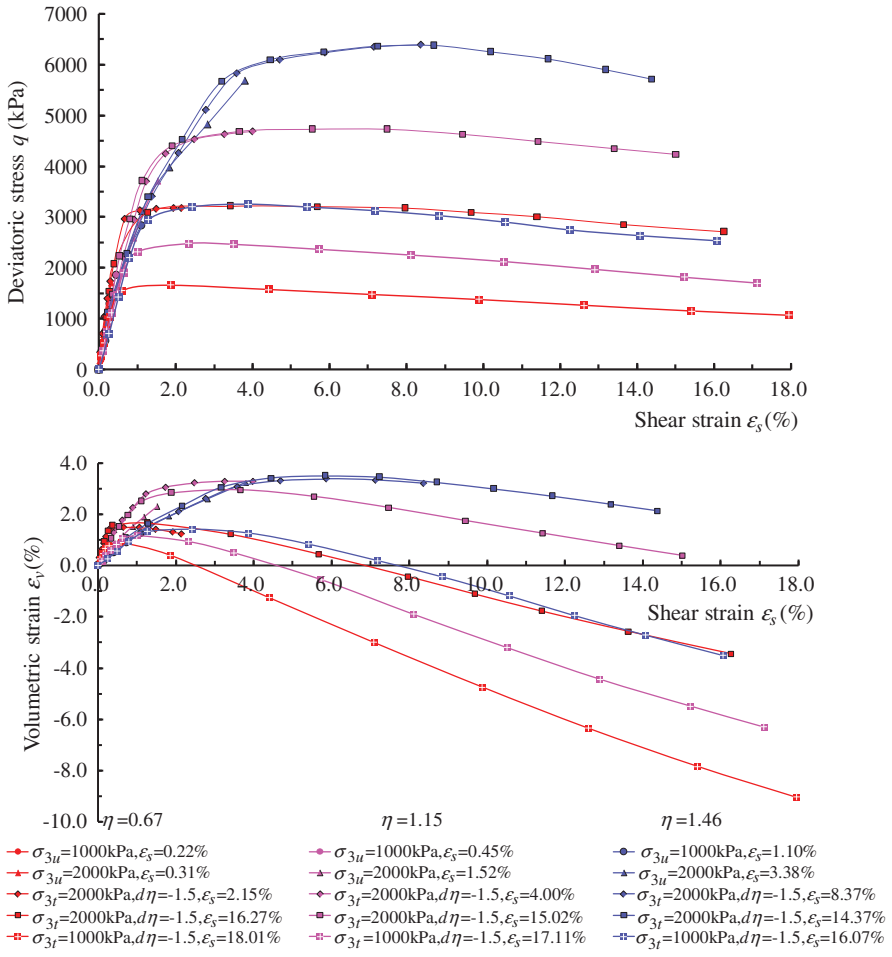

Fig. 11. (Color) Stress-strain curves under a transitional stress path of $d\eta = -1.5$.

Int. J. Geomech., 2019, 19(12): 04019124

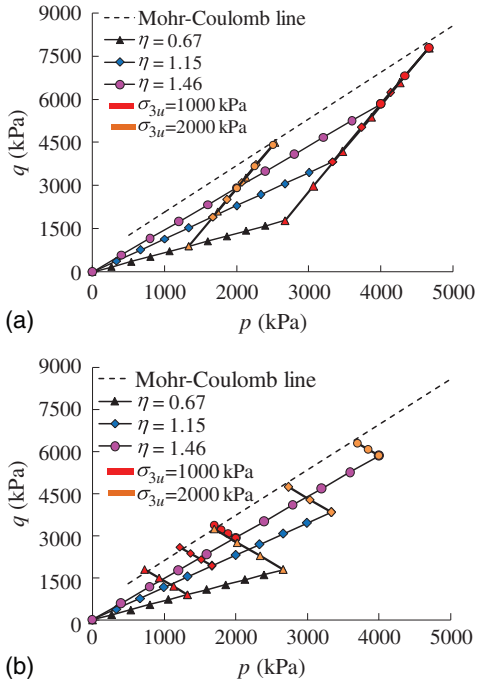

Fig. 12. (Color) Transitional stress paths for $d\eta$: (a) $d\eta = dq/dp = 3.0$; and (b) $d\eta = dq/dp = -1.5$.

Fig. 12 shows each stress path for the transitional stress path curves in Figs. 10 and 11. In Figs. 10–12 the stress-strain curves that experienced exactly or almost the same transitional stress path, such as the curves in Fig. 10, converged. This was also true for the curves under Loading paths 19 ($\eta = 0.67$, $\sigma_{3u} = 1{,}000$ kPa, $d\eta = -1.5$) and 26 ($\eta = 1.46$, $\sigma_{3u} = 1{,}000$ kPa, $d\eta = -1.5$) in Fig. 11—although these curves were obviously different before the transition. To analyze the changes in microstructure and their influence on stress-strain curves, Table 4 lists the gradations after each transitional stress path test.

Based on the gradations listed in Table 4, the relative breakage factors B_r under the transitional stress paths were calculated and are listed in Table 5; the corresponding volumetric strains ε_v, shear strains ε_s, and maximum deviatoric stresses q are also listed in Table 5. Fig. 13 shows the relationship between the B_r values from the table and ε_s under the transitional stress and conventional stress paths.

Fig. 13 shows that, under the transitional stress path, B_r increased with ε_s regardless of whether the stress ratio path $\eta = q/p$ equaled 0.67, 1.15, or 1.46, whether the transitional stress path $d\eta = dq/dp$ equaled 3.0 or -1.5, and whether the transitional confining pressure σ_{3t} equaled 1,000 or 2,000 kPa. This result was similar to the result under the conventional stress path. Furthermore, the growth rate of B_r under the transitional stress path increased with σ_{3t}, a result also similar to the result under the conventional stress path. Moreover, under the same transitional confining pressure, the growth rate of B_r under the transitional stress path $d\eta$ equaling 3.0 was higher than that under the path equaling -1.5. However, under the influence of $d\eta$, the B_r growth rate for the transitional stress paths experiencing the same equal stress ratio path showed obvious differences. For example, under the transitional stress path $d\eta$ of 3.0, the growth rate of B_r experienced by the equal stress ratio path η equaling 1.15 was higher than the others, while under the transitional stress path $d\eta$ of -1.5, the growth rate of B_r experienced by the equal stress ratio path η equaling 1.46 was the highest. Furthermore, under the transitional stress path $d\eta$ of -1.5, the growth rate of B_r was far lower than the rates under the equal stress ratio path, especially the B_r that experienced an equal stress ratio path η equaling 0.67, which exhibited a significantly different growth rate after the stress path transition.

The result just described was greatly different from that for the conventional stress path and indicated that particle breakage under the transitional stress path was totally different from that under the equal stress path. Thus, B_r and the corresponding shear strain ε_s, generated after the stress path transition, were calculated by B_r and ε_s under the transitional stress path (Table 5), deducing B_r and ε_s under the corresponding equal stress ratio path and transitional confining pressure (Table 1). Fig. 14 shows B_r and the corresponding ε_s generated after the stress path transition.

Table 4. Rockfill gradation after CD triaxial tests under transitional stress paths

	Particle amount (%) at each grain group (mm)								
Status	40–60	20–40	10–20	5–10	2–5	0.5–2.0	0.25–0.5	0.075–0.25	<0.075
After specimen preparation	21.17	34.85	18.87	11.33	7.43	4.19	1.13	0.37	0.66
Loading path No.									
9	14.17	32.03	22.62	13.10	9.95	4.92	1.55	0.64	1.02
10	7.46	34.52	22.65	13.85	10.68	6.23	1.96	0.98	1.67
11	13.10	34.28	22.73	12.68	9.47	4.71	1.51	0.63	0.89
12	12.86	33.14	23.05	12.11	9.98	5.23	1.64	0.7	1.29
13	9.37	31.55	22.98	13.02	12.16	6.27	2.04	1.04	1.57
14	12.25	34.19	22.95	13.15	9.21	4.74	1.59	0.62	1.30
15	12.84	32.51	23.23	12.68	9.97	5.28	1.66	0.71	1.12
16	8.66	34.31	20.63	13.47	12.24	6.26	1.96	1.02	1.45
17	12.67	34.17	23.16	12.67	9.36	4.80	1.55	0.63	0.99
18	18.42	34.80	21.58	11.46	7.76	3.96	1.15	0.34	0.53
19	17.71	34.35	21.31	11.97	7.94	4.21	1.29	0.48	0.74
20	20.11	33.74	20.64	11.66	7.65	4.06	1.19	0.40	0.55
21	15.40	35.30	22.52	11.55	8.66	4.08	1.22	0.47	0.80
22	14.68	35.35	21.00	12.53	9.00	4.43	1.46	0.61	0.94
23	19.19	33.35	21.49	11.55	7.91	4.12	1.27	0.44	0.68
24	13.33	34.36	22.48	12.31	9.63	4.87	1.50	0.61	0.91
25	13.11	32.11	23.17	12.79	9.69	5.30	1.70	0.79	1.34
26	17.17	33.38	22.25	12.20	8.24	4.24	1.31	0.51	0.70

Int. J. Geomech., 2019, 19(12): 04019124

Table 5. B_r under transitional stress paths

Loading path No.	η	$d\eta$	σ_{3t} (kPa)	B_r (%)	ε_v (%)	ε_s (%)	q (kPa)
9	0.67	3.0	2,000	4.07	4.17	7.49[a]	8,014
10	0.67	3.0	2,000	7.39	4.66	13.47	8,149
11	0.67	3.0	1,000	3.58	1.47	14.52	4,993
12	1.15	3.0	2,000	4.63	4.66	8.35[a]	7,812
13	1.15	3.0	2,000	7.67	5.13	13.30	8,019
14	1.15	3.0	1,000	4.22	1.33	14.56	4,609
15	1.46	3.0	2,000	4.66	4.59	8.98[a]	7,573
16	1.46	3.0	2,000	7.36	5.14	13.31	7,693
17	1.46	3.0	1,000	3.82	1.34	14.56	4,961
18	0.67	−1.5	2,000	0.49	1.25	2.15[a]	3,183
19	0.67	−1.5	2,000	1.36	−3.44	16.27	3,215
20	0.67	−1.5	1,000	0.38	−9.05	17.95	1,660
21	1.15	−1.5	2,000	1.85	3.30	4.00[a]	4,695
22	1.15	−1.5	2,000	2.81	0.41	15.02	4,730
23	1.15	−1.5	1,000	0.94	−6.30	17.12	2,480
24	1.46	−1.5	2,000	3.58	3.21	8.37[a]	6,398
25	1.46	−1.5	2,000	4.90	2.14	14.38	6,382
26	1.46	−1.5	1,000	1.73	−3.51	16.07	3,250

[a]Peak shear strength occurred.

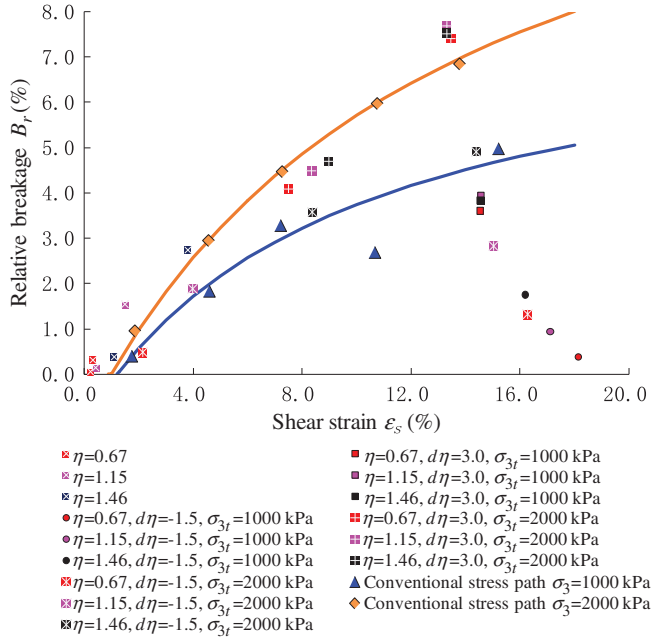

Fig. 13. (Color) B_r under transitional stress and conventional stress paths.

Fig. 14 shows that B_r generated after the stress path transition increased with shear strain ε_s and that the transitional stress path $d\eta = dq/dp$ and transitional confining pressure σ_{3t} influenced the growth rate. This result was similar to the result for B_r under the transitional stress path in Fig. 13. However, the experienced equal stress ratio η had a significant influence on the B_r growth rate, especially under a transitional confining pressure of 2,000 kPa, which was totally different from B_r under the transitional stress path in Fig. 13. Fig. 14 shows that, under the 2,000-kPa transitional confining pressure and the transitional stress path $d\eta$ of 3.0, the B_r growth rate increased as the experienced equal stress ratio η decreased. In contrast, under the 2,000-kPa transitional confining pressure and the transitional stress path $d\eta$ of −1.5, the B_r growth rate increased as the experienced equal stress ratio η increased. The plastic work was used to analyze this complex phenomenon.

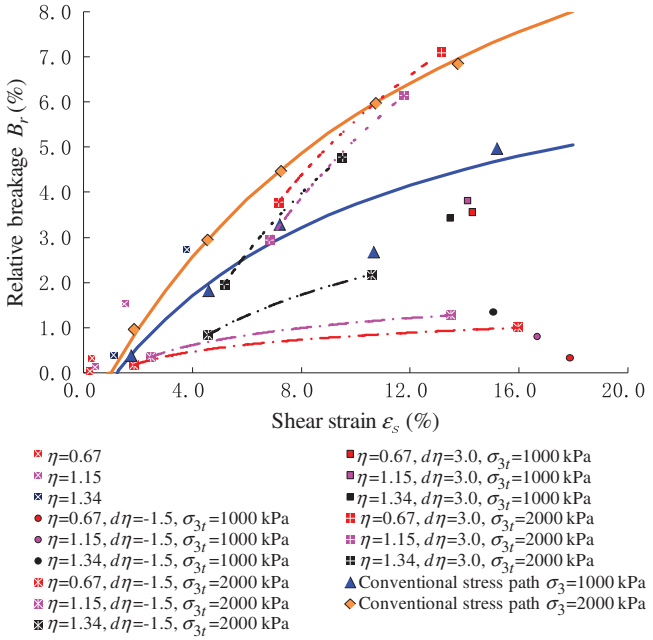

Fig. 14. (Color) B_r after stress path transition.

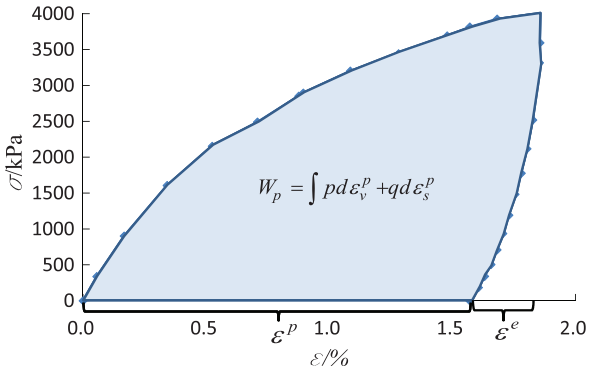

Fig. 15. (Color) W_p calculated using the stress-strain curve. (Reprinted from Jia et al. 2017, © ASCE.)

Particle Breakage from Plastic Work

Particle breakage is a process in which the work performed by the load is transformed into the surface energy of the new broken particles (Griffith 1921). Because it is a typically unrecoverable process, particle breakage was simulated using the plastic work in this study. Research has shown that the relationship between relative particle breakage factor B_r and plastic work under a conventional stress path can be simulated using a hyperbolic formulation (Jia et al. 2017; Liu et al. 2014). Hence, the plastic work W_p that corresponded to B_r in the tests was calculated according to the following formula:

$$W_p = \int pd\varepsilon_v^p + qd\varepsilon_s^p \tag{1}$$

where ε_v^p = plastic volumetric strain; and ε_s^p = plastic shear strain (Jia et al. 2017).

Fig. 15 shows the procedure that was used to calculate W_p with the stress-strain curve.

Fig. 16 shows the relationship between B_r and W_p under the equal stress ratio and transitional stress paths, meaning the stress

Int. J. Geomech., 2019, 19(12): 04019124

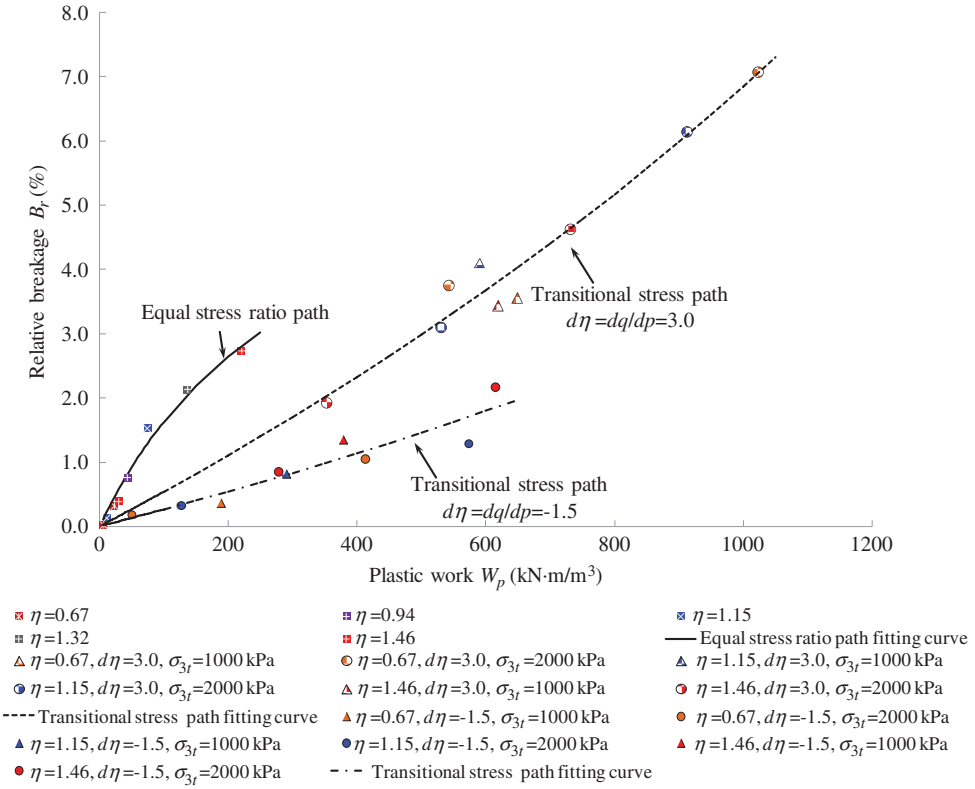

Fig. 16. (Color) B_r and W_p under equal stress and transitional stress paths.

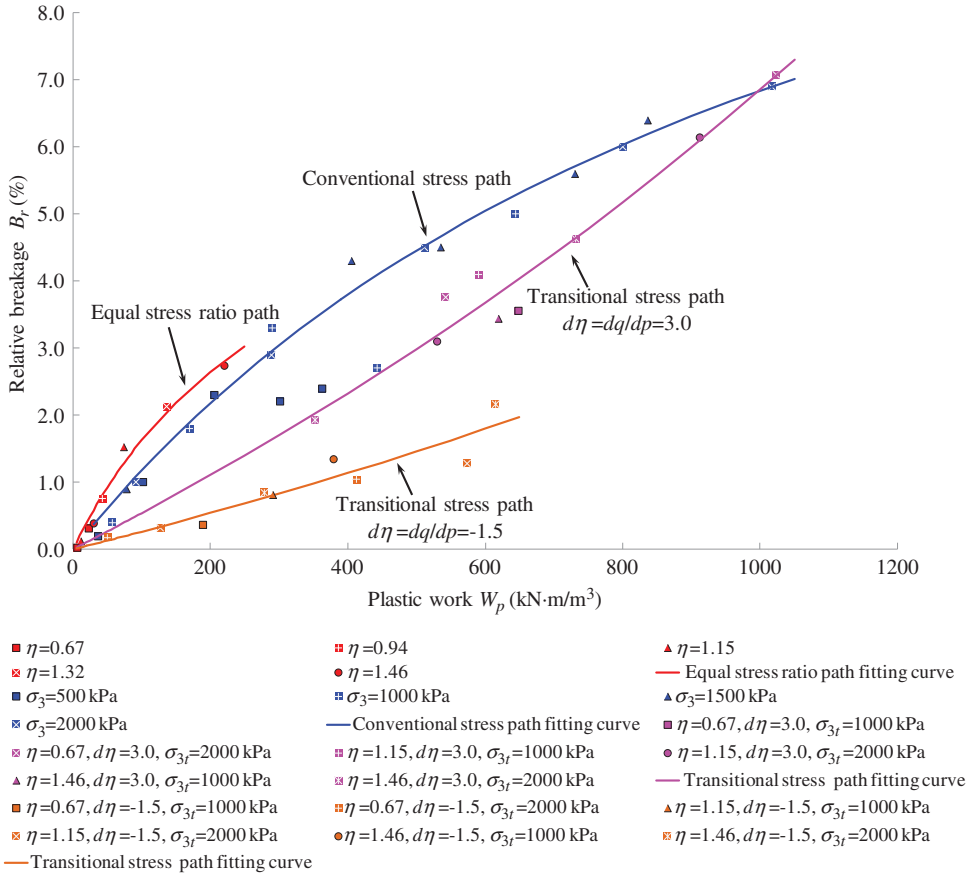

Fig. 17. (Color) B_r and W_p under different stress paths.

path after the transition. Fig. 16 shows that, under the equal stress ratio path and transitional stress path, all B_r values increased with W_p and that the increasing relationship obviously concentrated in three regions: B_r under the equal stress ratio path showed the highest growth rate, B_r under the transitional stress path $d\eta = 3.0$ showed the second highest rate, and B_r under the transitional stress path $d\eta = -1.5$ showed the lowest rate. In these regions, all specimens that experienced higher unloading confining pressure σ_{3u} or transitional confining pressure σ_{3t} (2,000 kPa) consumed larger W_p and generated higher B_r. Furthermore, under the equal stress ratio path, the specimens that experienced higher equal stress ratio η consumed larger W_p and generated higher B_r. This phenomenon also appeared in the specimens under the transitional stress path of −1.5. However, under the transitional stress path of 3.0, the specimens that experienced lower stress ratio η consumed larger W_p and generated higher B_r. The difference in the B_r–W_p relationship between the transitional stress paths of 3.0 and −1.5 was similar to the difference in the B_r–ε_s relationship in Fig. 14. This result indicated that, under the 2,000-kPa transitional confining pressure and the 3.0 transitional stress path, the particles were effectively limited and loaded to similar failure stress, which adequately released the particle breakage potential of each specimen. Therefore, the specimens that experienced lower equal stress ratio η and generated less particle breakage before the stress path transition had greater particle breakage potential and generated more particle breakage, consuming more plastic work. Under the −1.5 transitional stress path, the decreased confining pressure could not limit the particles' sliding and rolling over. The specimens that experienced higher equal stress ratio η generated more particle breakage, resulting in a seriously damaged structure before the transition. Then, after the transition, these specimens also underwent higher failure deviatoric stress, generated greater particle breakage, and consumed more plastic work.

Fig. 17 shows B_r and W_p under the conventional stress path (Jia et al. 2017), equal stress ratio path, and transitional stress path. The relationship between B_r and W_p under each stress path was simulated according to the following hyperbolic formulation:

$$B_r = \frac{W_p}{A + B \times W_p} \tag{2}$$

where A and B = fitting parameters (Jia et al. 2017).

Table 6 lists the fitting parameters under each stress path. Fig. 17 and Table 6 show that the relationship between B_r and W_p under the conventional stress path was similar to that under the equal stress ratio path and was obviously different from that under the transitional stress path.

Fig. 17 and Table 6 show that, under the equal stress ratio path, the B_r growth rate was higher than that under the conventional stress path, indicating that, under the equal stress ratio path, the rockfill particles were easily broken and consumed less plastic work. This result occurred because the rockfill particles under the equal stress ratio path did not experience as much consolidation as those under the conventional stress path before shearing and could not form a stable skeleton. Furthermore, the confining pressure under the equal stress ratio path increased continuously and limited particle sliding and rollover. Therefore, the rockfill particles under the equal stress ratio path had fewer contacts and experienced larger contact forces, resulting in more particle breakage and volumetric deformation. Fig. 18 shows the stress-strain curves under the conventional stress and transitional stress paths, illustrating that volumetric deformation under the equal stress ratio path before the stress path transition was much greater than that under the conventional stress path.

Table 6. Fitting parameters under each stress path

Stress path	A	B
Equal stress ratio	4,726	14.2
Conventional stress	7,816	6.8
Transitionalstress = 3.0	18,929	−4.3
Transitionalstress = −1.5	38,761	−8.9

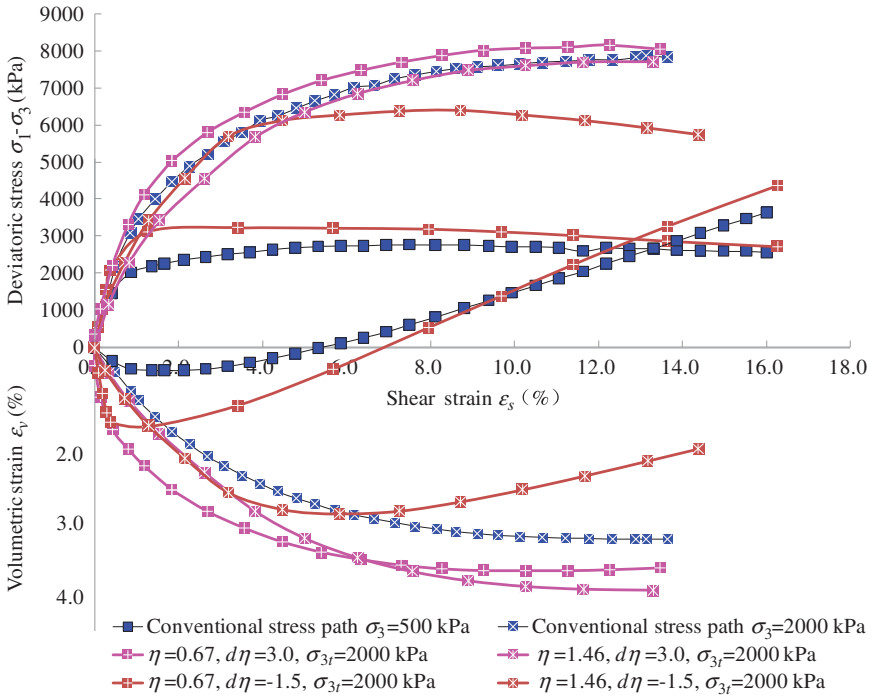

Fig. 18. (Color) Stress-strain curves under different stress paths.

Int. J. Geomech., 2019, 19(12): 04019124

Fig. 17 shows that, under the transitional path $d\eta$ of 3.0, the B_r growth rate was lower than that under the conventional stress path because, under the equal stress ratio path before the transition, more particle breakage appeared than under the conventional stress path, which also adjusted the material to a difficult breakage particle gradation. Therefore, the B_r growth rate under the transitional stress path that experienced an equal stress ratio of 0.67 and presented less particle breakage before the transition was closer to the conventional stress path than the other transitional stress path was. Moreover, the rockfill particles under the transitional stress path were not sufficiently consolidated, so they had more space for sliding and skeleton adjustment than they did under the conventional stress path, which generated larger volumetric strain (as Fig. 18 shows) and consumed more plastic work.

Fig. 17 shows that, under the transitional path $d\eta$ of -1.5, the B_r growth rate was the lowest. Fig. 18 shows that, under the transitional path $d\eta$ of -1.5, the volumetric strain curves exhibited significant dilatancy and were similar to the curves for the conventional stress path under a confining pressure of 500 kPa, which also had a much lower B_r growth rate than the confining pressure under the conventional stress path. These results led to the conclusion that the large dilatancy decreased the plastic work consumed by particle breakage, which appeared in the former conventional stress path tests (Jia et al. 2017).

Particle breakage under the transitional stress, equal stress ratio, and conventional stress paths (Jia et al. 2017) indicated that the conventional stress path was a special transitional stress path that experienced an equal stress ratio η of zero. Under the equal stress ratio path, particle breakage increased with shear strain and the growth rate of particle breakage increased. Additionally, once the equal stress ratio path η equaled zero, the particle breakage growth ratio approached infinity and the shear strain equaled zero. Thus, little particle breakage appeared in the consolidation test (Jia et al. 2017). Under the transitional stress path (the stress path after the transition), particle breakage increased with shear strain and the growth rate was influenced by the transitional confining pressure, the transitional stress path, and the experienced equal stress ratio before the transition. The stress path significantly influenced the relationship between B_r and W_p. The hyperbolic formulation could not reasonably simulate the relationship between B_r and W_p under the transitional stress path.

Conclusions

In this paper, a series of triaxial tests using basalt rockfill from the Gushui CFRD under complex stress paths were performed to investigate rockfill particle breakage. The main conclusions are summarized as follows:

- The stress path has a significant influence, similar to the influence of stress state and shear strain, on rockfill particle breakage. Under the equal stress ratio path, relative particle breakage factor B_r increases with shear strain ε_s and the growth rate decreases as the stress ratio $\eta = q/p$ increases.
- Under the equal stress ratio path, no particle breakage occurs in a part of the shear strain (marked ε_{si}) at the beginning of loading, which also appears in the conventional stress path (Jia et al. 2017); ε_{si} decreases with η.
- The conventional stress path (consolidated drained triaxial compression test) is a special transitional stress path, with an equal stress ratio η of zero and a transitional stress path $d\eta = dq/dp$ of 3.0. Under the zero-stress ratio path, the particle breakage growth rate approaches infinity and the shear strain equals zero. Thus, little particle breakage appeared in the consolidation test.
- Under the transitional stress path, the relative particle breakage factor B_r increases with shear strain ε_s and the growth rate is influenced by the transitional confining pressure σ_{3t}, the transitional stress path $d\eta$, and the equal stress ratio η experienced before the transition.
- Under the complex stress path, the relative particle breakage factor B_r increases with plastic work W_p in a relationship similar to that under the conventional stress path. Under the equal stress ratio path, the relationship between B_r and W_p can be simulated using a hyperbolic formulation. However, under the transitional stress path, B_r cannot be reasonably simulated using W_p.

Acknowledgments

This research was supported by the National Key Research and Development Plan (Grant No. 2016YFB0201001) and the National Natural Science Foundation of China (Grant Nos. 51379029, 51679029, 51109027, and 51179024).

Notation

The following symbols are used in this paper:

A = fitting parameter;
B = fitting parameter;
B_r = relative breakage factor;
P = mean effective stress;
q = deviatoric stress;
W_p = plastic work;
ε^p = plastic strain;
ε_v^p = plastic volumetric strain;
ε_s = shear strain;
ε_{si} = shear strain in which no particle breakage occurs;
ε_s^p = plastic shear strain;
ε_v = volumetric strain;
η = stress ratio;
σ = p or q;
σ_3 = confining pressure;
σ_{3t} = transitionl confining pressure; and
σ_{3u} = unloading confining pressure.

References

Bai, S., X. Zhou, and H. Chao. 1999. "Effects of stress path on the deformation of rockfill materials." [In Chinese.] *Shuili Fadian Xuebao/J. Hydroelectric Eng.* 4 (Jan): 76–80.

Chang, D. S., and L. Zhang. 2013. "Critical hydraulic gradients of internal erosion under complex stress states." *J. Geotech. Geoenviron. Eng.* 139 (9): 1454–1467. https://doi.org/10.1061/(ASCE)GT.1943-5606.0000871.

Charles, J. A. 1976. "Use of one-dimensional compression tests and elastic theory in predicting deformations of rockfill embankments." *Can. Geotech. J.* 13 (3): 189–200. https://doi.org/10.1139/t76-023.

Chavez, C., and E. E. Alonso. 2003. "A constitutive model for crushed granular aggregates which includes suction effects." *Soils Found.* 43 (4): 215–227. https://doi.org/10.3208/sandf.43.4_215.

Chen, Q., B. Indraratna, J. P. Carter, and S. Nimbalkar. 2016. "Isotropic kinematic hardening model for coarse granular soils capturing particle breakage and cyclic loading under triaxial stress space." *Can. Geotech. J.* 53 (4): 646–658. https://doi.org/10.1139/cgj-2015-0166.

Feng, W., C. Shichun, L. Shijie, and J. Yufeng. 2016. "Testing and micromechanical modelling of rockfill materials considering the effect of stress path." *Math. Probl. Eng.* 2016. https://doi.org/10.1155/2016/7630541.

Griffith, A. A. 1921. "The phenomena of rupture and flow in solids." *Philos. Trans. R. Soc. London, Ser. A* 221 (1921): 163–198. https://doi.org/10.1098/rsta.1921.0006.

Guo, X., H. Hu, and C. Bao. 1997. "Experimental studies of the effects of grain breakage on the dilatancy and shear strength of rock fill." [In Chinese.] *Yantu Gongcheng Xuebao/Chin. J. Geotech. Eng.* 19 (3): 83–88.

Hardin, B. O. 1985. "Crushing of soil particles." *J. Geotech. Eng.* 111 (10): 1177–1192. https://doi.org/10.1061/(ASCE)0733-9410(1985)111:10(1177).

Indraratna, B., N. T. Ngo, and C. Rujikiatkamjorn. 2013. "Deformation of coal fouled ballast stabilized with geogrid under cyclic load." *J. Geotech. Geoenviron. Eng.* 139 (8): 1275–1289. https://doi.org/10.1061/(ASCE)GT.1943-5606.0000864.

Jia, Y., B. Xu, S. Chi, B. Xiang, and Y. Zhou. 2017. "Research on the particle breakage of rockfill materials during triaxial tests." *Int. J. Geomech.* 17 (10): 04017085. https://doi.org/10.1061/(ASCE)GM.1943-5622.0000977.

Liu, H., D. Zou, and J. Liu. 2014. "Constitutive modeling of dense gravelly soils subjected to cyclic loading." *Int. J. Numer. Anal. Methods Geomech.* 38 (14): 1503–1518. https://doi.org/10.1002/nag.2269.

Liu, J., D. Zou, and X. Kong. 2018. "Three-dimensional scaled memory model for gravelly soils subject to cyclic loading." *J. Eng. Mech.* 144 (3): 04018001. https://doi.org/10.1061/(ASCE)EM.1943-7889.0001367.

Marachi, N., C. Chan, and H. Seed. 1972. "Evaluation of properties of rockfill materials." *J. Soil Mech. Found. Div.* 98 (1): 95–114. https://doi.org/10.1061/(ASCE)EM.1943-7889.0001367.

Marsal, R. J. 1967. "Large scale testing of rockfill materials." *J. Soil Mech. Found. Div.* 93 (2): 27–43.

McDowell, G. R. 2003. "Micromechanics of creep of granular materials." *Geotechnique* 53 (10): 915–916. https://doi.org/10.1680/geot.2003.53.10.915.

McDowell, G. R., and M. D. Bolton. 1998. "On the micromechanics of crushable aggregates." *Geotechnique* 48 (5): 667–679. https://doi.org/10.1680/geot.1998.48.5.667.

Newland, P. L., and B. H. Allely. 1959. "Volume changes during undrained triaxial tests on saturated dilatant granular materials." *Geotechnique* 9 (4): 172–184. https://doi.org/10.1680/geot.1959.9.4.174.

Ng, C. W. W., W. T. Fung, C. Y. Cheuk, and L. Zhang. 2004. "Influence of stress ratio and stress path on behavior of loose decomposed granite." *J. Geotech. Geoenviron. Eng.* 130 (1): 36–44. https://doi.org/10.1061/(ASCE)1090-0241(2004)130:1(36).

Ng, T. T. 2005. "Behavior of gravity deposited granular material under different stress paths." *Can. Geotech. J.* 42 (6): 1644–1655. https://doi.org/10.1139/t05-080.

Oldecop, L. A., and E. E. Alonso. 2001. "A model for rockfill compressibility." *Geotechnique* 51 (2): 127–139. https://doi.org/10.1680/geot.2001.51.2.127.

Qin, S. L., L. Q. Yang, H. Gao, and S. X. Chen. 2015. "Acoustic emission characteristics of sericite schist coarse aggregates under different stress paths." [In Chinese.] *Yantu Lixue/Rock Soil Mech.* 36 (1): 89–96.

Salim, W., and B. Indraratna. 2004. "A new elastoplastic constitutive model for coarse granular aggregates incorporating particle breakage." *Can. Geotech. J.* 41 (4): 657–671. https://doi.org/10.1139/t04-025.

Sun, Q. D., B. Indraratna, and S. Nimbalkar. 2014. "Effect of cyclic loading frequency on the permanent deformation and degradation of railway ballast." *Geotechnique* 64 (9): 746–751. https://doi.org/10.1680/geot.14.T.015.

Wang, G. J., C. H. Yang, C. Zhang, H. J. Mao, and W. Wang. 2009. "Experimental research on particle breakage and strength characteristics of rock and soil materials with different coarse-grain contents." [In Chinese.] *Yantu Lixue/Rock Soil Mech.* 30 (12): 3649–3654.

Wei, K. 2012. "Study on collapse behaviors of coarse grained soils." *Periodica Polytech.-Civ.* 56 (2): 245–252. https://doi.org/10.3311/pp.ci.2012-2.11.

Wei, S., and J. Zhu. 2006. "Study on wetting breakage of coarse-grained materials in triaxial test." [In Chinese.] *Yanshilixue Yu Gongcheng Xuebao/J. Hydraul. Eng.* 25 (6): 1252–1258.

Xiang, B., Z. L. Zhang, and S. C. Chi. 2009. "An improved hypoplastic constitutive model of rockfill considering effect of stress path." *J. Cent. South Univ.* 16 (6): 1006–1013. https://doi.org/10.1007/s11771-009-0167-3.

Xiang, B., Z. L. Zhang, S. C. Chi, and G. Lin. 2010. "Study of constitutive relations of rockfill under complex stress path." [In Chinese.] *Yantu Lixue/Rock Soil Mech.* 31 (6): 1716–1723.

Xiao, Y., H. Liu, Y. Chen, and J. Jiang. 2014. "Strength and deformation of rockfill material based on large-scale triaxial compression tests. I: Influences of density and pressure." *J. Geotech. Geoenviron. Eng.* 140 (12): 04014070. https://doi.org/10.1061/(ASCE)GT.1943-5606.0001176.

Xiao, Y., H. Liu, C. S. Desai, Y. Sun, and H. Liu. 2016. "Effect of intermediate principal-stress ratio on particle breakage of rockfill material." *J. Geotech. Geoenviron. Eng.* 142 (4): 06015017. https://doi.org/10.1061/(ASCE)GT.1943-5606.0001433.

Xiao, Y., H. Liu, J. Zhu, and W. Shi. 2011. "Dilatancy equation of rockfill material under the true triaxial stress condition." Supplement, *Sci. China Technol. Sci.* 54 (S1): 175–184. https://doi.org/10.1007/s11431-011-4636-1.

Yang, G., X. Sun, Y. Z. Yu, and B. Y. Zhang. 2010a. "Experimental study of mechanical behavior of a coarse-grained material under various stress paths." [In Chinese.] *Yantu Lixue/Rock Soil Mech.* 31 (4): 1118–1122.

Yang, G., B. Y. Zhang, Y. Z. Yu, and X. Sun. 2010b. "An experimental study on particle breakage of coarse-grained materials under various stress paths." [In Chinese.] *Shuili Xuebao/J. Hydraul. Eng.* 41 (3): 338–342.

Yuan, W., Z. Sheng, A. Da-hua, Y. yu-zhen, and S. Xun. 2017. "Particle breakage characteristics of rockfills under complex stress paths." [In Chinese.] *Chin. J.Geotech. Eng.* 40 (4): 698–706.

Zhang, B. Y., J. H. Zhang, and G. L. Sun. 2012. "Particle breakage of argillaceous siltstone subjected to stresses and weathering." *Eng. Geol.* 137–138 (Jun): 21–28. https://doi.org/10.1016/j.enggeo.2012.03.009.

Zhang, B. Y., J. H. Zhang, and G. L. Sun. 2015. "Deformation and shear strength of rockfill materials composed of soft siltstones subjected to stress, cyclical drying/wetting and temperature variations." *Eng. Geol.* 190 (May): 87–97. https://doi.org/10.1016/j.enggeo.2015.03.006.

Zhu, S., Y. Wang, S. Feng, and C. Zhong. 2010. "Comparison and study on constitutive models for coarse grained materials under different stress path." In *Proc., 12th Int. Conf. on Engineering, Science, Construction, and Operations in Challenging Environments—Earth and Space 2010*, 423–430. Reston, VA: ASCE.